A Novel Empirical Orthogonal Function (EOF)-Based Methodology to Study the Internal Wave Effects on Acoustic Propagation

Gaëlle Casagrande, Yann Stéphan, Alex C. Warn Varnas, and Thomas Folegot

Abstract—This paper presents a novel approach to synthesize realistic environment for ocean-acoustic parametric studies. In its current form, this methodology applies to internal waves and tides. Empirical orthogonal function (EOF) decomposition is applied to a temporal series of temperature profiles. It can be observed that the first two time-dependent expansion coefficients are dynamically linked. When they are plotted one versus another in a scatter diagram, the cloud of points consists of a crescent shape that can easily be represented by a polynomial fit. If the first two expansion coefficients capture enough variability in the temperature profiles, the EOF modes plus the polynomial can be used to reconstruct temperature profiles independently from the set of data. This realistic synthesized environment can then be input to acoustic propagation models. This approach is applied to the case of the Messina Strait in which internal waves are known to be intensive. From a short-term series of temperature profiles collected on a thermistor string, range-dependent profiles along and across the strait are reconstructed. The acoustical impact study is conducted with the range-dependent acoustic model (RAM) parabolic equation (PE) model. The methodology presented in this paper is simple to run and requires a very affordable set of data. It could be used as an efficient alternative to ocean and acoustic model coupling for process studies or for regional studies especially in poorly known areas or highly variable areas, where it is difficult to obtain good sound-speed profile prediction from ocean models.

Index Terms—Empirical orthogonal function (EOF), internal waves, Messina Strait, ocean-acoustics modeling.

I. INTRODUCTION

INTERNAL WAVES (IW) are known to have a significant impact on the acoustic propagation (e.g., [1] and [2]). From a geometrical point of view, the vertical displacements of the thermocline can modify drastically the surface duct and can also locally modify the conditions of propagation if the acoustic source or receivers are placed in this critical layer [3]. From an energetic point of view, the acoustic propagation through IW can also induce focusing effects [4]. Anticipating the effects of internal waves in a region of interest, whether scientific or military, is then highly interesting for tomographers and oceanographers, who may want to design and optimize inversion schemes or for sonar operators and decision makers who may want to optimize antisubmarine warfare (ASW) tactics and behaviors in IW fields.

The impact of IW can be numerically studied coupling IW models and ocean-acoustic propagation models. Such studies can be separated into two categories: process studies and regional studies. As far as process studies are concerned, the purpose is generally to conduct a parametric study of the impact of IW in a set of acoustic scenarios. For that purpose, simplified IW models can be used as feature models, relying on a mathematical description of the IW or process models, numerically resolving the underlying physics of the generation and propagation of IW, whereas in regional studies, the aim is to provide a realistic environment in which IW is only a contribution. For that purpose, regional general circulation models can be used provided they can account for IW predictions.

We propose in this paper a novel approach which can be considered as a compromise approach between process modeling and regional modeling. The motivation of this work is indeed to have a simple efficient way to build realistic environments when one wants to focus on a particular phenomenon in a particular region. Our approach is data driven but does not require a full knowledge of the region of interest. On the other hand, our approach is also parametric but does not require a too complicated process model or a too simple parametric model. The method proposed in this paper relies on the decomposition of a simple set of data (in practical, a short-term temporal series of temperature profiles) into empirical orthogonal functions (EOFs). It has been shown in [5] that in the case of IW in the Messina Strait, the time-varying expansion coefficients of the first two EOFs represent over 99% of the variance and are dynamically linked. When plotting the expansion coefficients one versus the other, the scatter diagram has a well-defined crescent shape. This feature is confirmed by EOF analysis of numerical outputs from the Lamb model [6]. The signature of internal waves in EOF expansion coefficient scatter diagrams can then be used to detect the presence of internal waves in regions of the ocean. A curve can be fitted to the crescent-shaped scatter diagram in presence of internal waves. Such a curve could be derived for various regions. This led to building a representation

G. Casagrande is with the French Armament Procurement Agency (DGA), Bagneux 92221, France (e-mail: gaelle.casagrande@dga.defense.gouv.fr).

Y. Stéphan is with the Service Hydrographique et Océanographique de la Marine (SHOM), Brest 29200, France (e-mail: yann.stephan@shom.fr).

A. W. Varnas is with the Naval Research Laboratory, Stennis Space Centre, MS 39529 USA (e-mail: varnas@nrlssc.navy.mil; alex.warnvarnas.ctr@nrlssc.navy.mil; kazysvarnas@gmail.com).

T. Folegot is with Quiet Oceans, Plouzané 29280, France (e-mail: folegot@quiet-oceans.com).
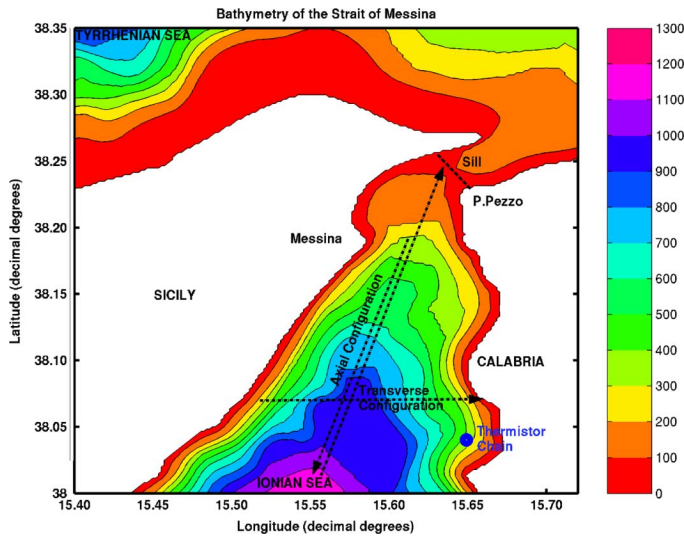
Fig. 1. Bathymetry of the Strait of Messina; the color bar indicates the depths in meters. The blue dot represents the position of the thermistor string. The dotted lines correspond to the axis of simulations in the two acoustic configurations. For the transverse configuration, the source is located close to the Sicilian coast and emits towards the Italian coast. For the axial configuration, the source was positioned either in front of Messina and emitting southwards (downslope configuration), or at the south part of the strait and emitting towards the sill (upslope configuration).

of internal wave events with no more that a statistically pertinent set of data. A parametric study enables to reconstruct a set of plausible range-dependent environments which account for the actual variability in the considered region. By applying an acoustic propagation loss model, it is then possible to anticipate the acoustical impact. This novel methodology is applied to a data set from the COACH'06 experiment jointly conducted in November 2006 by the NATO Undersea Research Centre (NURC) and the Service Hydrographique et Océanographique de la Marine (SHOM).

In the first part of this paper, we recall the data set and describe the variability in terms of EOF decomposition. We then describe the method to reconstruct the synthetic environments. To illustrate our approach, the third part presents a parametric acoustical study of the effect of IW in the Strait of Messina using the variability obtained by EOF decomposition. Conclusions and perspectives are drawn in the last part of the paper.

II. DATA AND STATISTICAL ANALYSIS

A. Preliminary Consideration on the Strait of Messina

The Strait of Messina is a rich dynamic area where many ocean features can be encountered. It separates the Italian Peninsula from the island of Sicily and is a natural connection between the Tyrrhenian Sea in the north and the Ionian Sea in the south. The strait is a narrow channel, whose smallest cross-sectional area is 0.3 km^2 in the sill region. There, the mean water depth is 80 m (Fig. 1). The water depth increases gently in the northern part and rapidly in the southern basin. Throughout the year, two water masses are encountered in the strait: the Tyrrhenian Surface Water (TSW) and the colder and saltier Levantine Intermediate Water (LIW).

Although tidal displacements are very small in the strait of Messina (the order of 10 cm), the tidal phase opposition between the two basins can lead to a sea surface slope of 1–2 cm km^{-1} thus generating very strong currents as high as 3 m s^{-1} in the sill region during spring tides [7], [8]. The strong barotropic tidal flow over a steep bathymetry in a stably stratified environment represents the ideal recipe for internal wave generation [9]. Baines [10], [11] has demonstrated the generation process analytically. The hydrodynamic modeling of tidal flow over steep topography shows that the tidal flow creates an interfacial depression of the pycnocline and generates an internal baroclinic bore at the sill during maximum flows in a tidal cycle ([12], [6], [13], [1], [2], [14]. In the Strait of Messina, during *rema montante* when the heavier LIW crosses the sill, the pycnocline is moved upwards at the sill and depressed in the north basin. The depression is an internal bore that generates a southwards and a northwards propagating internal wave. The northwards propagating bore steepens and disintegrates into solitary waves whereas the southwards propagating bore is stopped by the sill. When the semidiurnal tide reverses to *rema scendente*, the southwards propagating internal bore of depression undergoes a hydraulic jump over the sill and into the southern basin where it propagates away from the sill. As it propagates, nonlinear effects steepen its leading edge until it disintegrates into a series, or "train," of interfacial nonlinear short internal waves because of frequency and amplitude dispersions. The process is very well described in [2]. The characteristics for internal waves in the Strait of Messina are a propagation speed between 0.80 and 1.00 m s^{-1}, with oscillations up to 2 °C amplitude (20–50 m). When the train of internal waves is well formed, 4–10 periods ranging from 8 to 30 min can be observed, covering an average total duration of 2 h [7].

B. Presentation of the Oceanographic Data

One thermistor chain was bottom-moored about 27 km south of the sill of strait (Fig. 1), at location (15°38′57″ E, 38°02′24″ N) from November 4, 2006 16:48:00 UTC to November 7, 2006 07:12:00 UTC, with a 1-min temporal resolution which allows clean observations of internal solitary wave events. It had ten sensors positioned from 14- to 128-m depth.

Fig. 2 shows the temperature measured by the thermistor string. The thermocline depth stands around 95 m for the first day and half, and raises slowly to a 60-m depth after November 6, 2006. The deepening of warm surface waters illustrates the occurrence of internal solitary wave train events every half day. After November 6, 2006, the mean pycnocline depth goes up by 30 m, most likely due to some wind event relaxation (hypothesis, no meteorological data).

Table I summarizes precisely the occurrence of the internal wave trains (IWTs) observed on the thermistor string data and the reversal of the tide from *rema montante* (northwards) to *rema scendente* (southwards). It shows that IWTs are visible 6 h after the tide reversal from North to South. If considering the hypothesis made by [7] that the internal bores are generated at slack waters when the flow reverses from north to south (for southwards propagating internal solitary waves), then the average speed of the IWTs here is 1.25 m s^{-1}. The amplitudes of the internal solitary waves range between 40 and 50 m. The
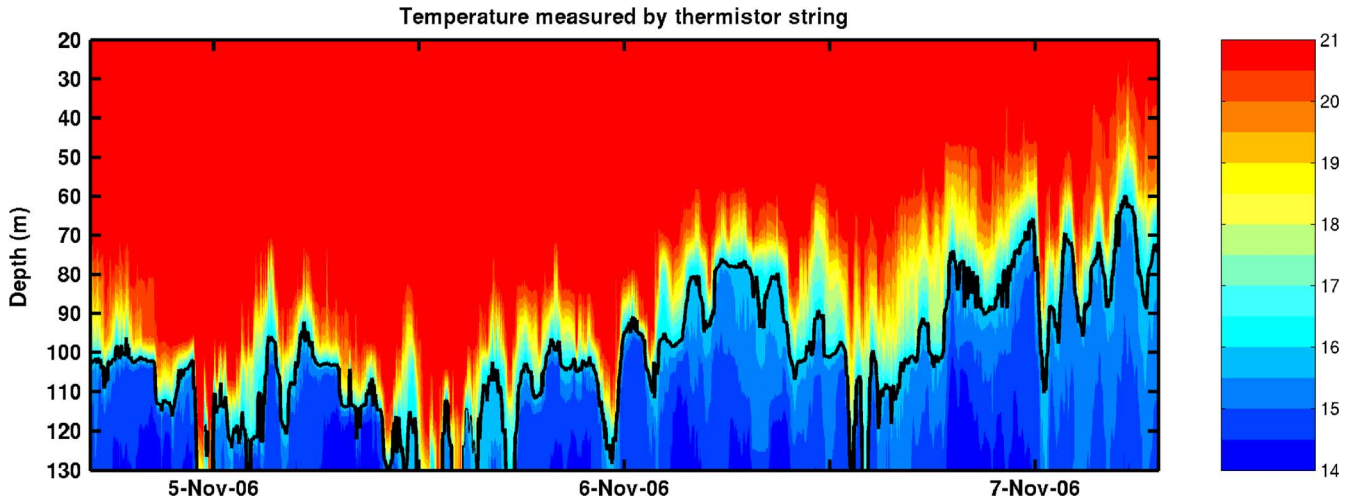
Fig. 2. Thermistor string measured temperature from November 4, 2006 16:48:00 UTC to November 7, 2006 07:12:00 UTC. The color bar displays the temperature in degrees Celsius. The 16 °C temperature contour is plotted to underline the temperature variability due to occurrence of internal waves.

Table I

INTERNAL WAVE TRAINS (IWT) IDENTIFIED ON THE THERMISTOR STRING MEASUREMENT. AS THE BORE GENERATED AT "REMA MONTANTE" ON THE NORTHERN SIDE OF THE STRAIT UNDERGOES A HYDRAULIC JUMP OVER THE SILL TO THE SOUTHERN BASIN WHEN THE TIDE REVERSES SOUTHWARDS (REMA SCENDENTE), THE TIME DIFFERENCE BETWEEN THE SAR IMAGE AND THE TIDAL REVERSAL IS COMPUTED IN ORDER TO GET THE PROPAGATION SPEED OF THE IWT IN THE SOUTH BASIN. THE FIRST LINE INDICATES THE DATE AND TIME OF THE IWT EVENT, AND THE SECOND LINE INDICATES THE TIME OF TIDAL REVERSAL FROM NORTH TO SOUTH (SLACK WATERS) PREVIOUS TO THE SAR IMAGE. THE LAST LINE SHOWS THE TIME DIFFERENCE BETWEEN THE PREVIOUS TIDE REVERSAL AND THE OCCURRENCE OF THE IWT

Internal Wave Trains	IWT 1	IWT 2	IWT 3	IWT 4	IW 5
Occurrence of IWT	Nov. 4th 2006 23:31 UTC	Nov. 5th 2006 11:55 UTC	Nov. 5th 2006 23:40 UTC	Nov. 6th 2006 13:15 UTC	Nov. 7th 2006 00:15 UTC
Previous tide reversal (slack waters)	Nov. 4th 2006 17:02 UTC	Nov. 5th 2006 06:05 UTC	Nov 5th 2006 17:39 UTC	Nov. 6th 2006 06:48 UTC	Nov. 6th 2006 18:14 UTC
Δt (REV - IWT)	6:29	5:50	6:01	6:27	6:01

trains have two to four internal solitary waves. The first and second ones are very neat in the data.

C. Theory of the EOF Analysis

The EOF decomposition, also called principal component analysis, is one of a larger class of inverse techniques and is equivalent to a data reduction method [15]. It is one of the most powerful methods for reducing the variability in the data into a few patterns. It provides a compact description of the spatial and temporal variability of data series in terms of orthogonal functions, or statistical "modes," resulting from the decomposition of the data signal in eigenvalues and eigenvectors. Each set of eigenvector, called EOF mode, represents a standing oscillation pattern [16]. The eigenvalues are normalized and ordered according to their size to indicate what EOF mode contains more variance. Therefore, each eigenvalue is associated with a pattern, giving a measure of the fraction of the total variance explained by each EOF mode. The projection of the data onto the standing EOF modes, called principal component time series (PC) or expansion modes of the EOFs, gives an estimate of how the pattern oscillates in time. Most of the variance is usually in the first few orthogonal functions. However, one must be careful before making any physical assumption on

the mechanism of a phenomenon. As the method finds a set of orthonormal basis vectors that maximizes the projection of the data on the basis vectors, the EOF modes are uncorrelated over space and the expansion coefficients are uncorrelated over time. Thus, these patterns of variability are primarily "data" modes and not necessarily "physical" modes [17].

In this paper, the EOF analysis was applied on the vertical to the temperature anomaly (the work was done on the density anomaly in [5]), so that the measured temperature $\psi(z,t)$ could be written as

$$\psi(z,t) = \bar{\psi}(z) + \sum_{i=1}^{M} \alpha_i(t) \cdot \phi_i(z) \qquad (1)$$

where $\bar{\psi}(z)$ is the time-averaged vertical temperature profile, M is the number of considered EOF, $\alpha_i(t)$ is the amplitude of the ith orthogonal mode at time t, and $\phi_i(z)$ is the ith EOF. This equation says that the time variation of the dependent scalar variable $\psi(z,t)$ at each depth results from the linear combination of M spatial functions ϕ_i, whose amplitudes are weighted by M time-dependent coefficients $\alpha_i(t)$. The weights $\alpha_i(t)$ tell how the spatial modes ϕ_i vary with time. As there are many terminologies for EOF analysis, we insist on the fact that the use of
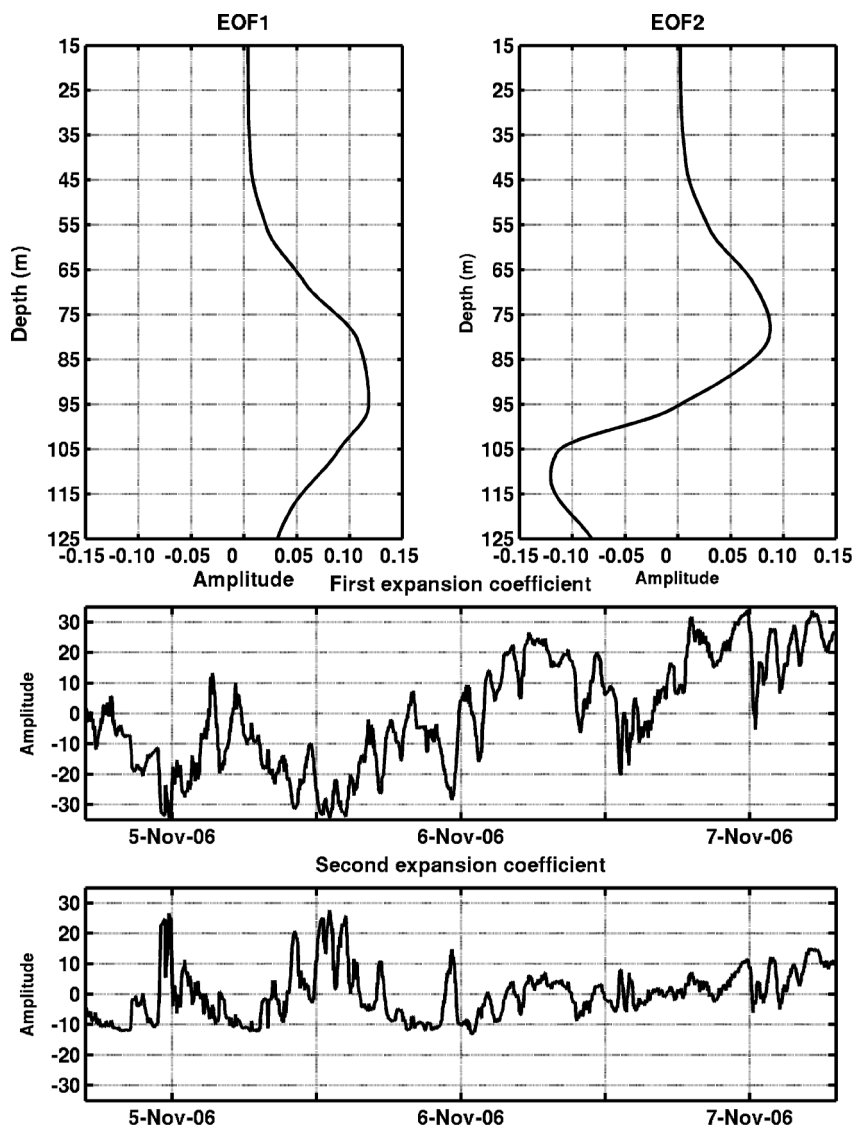
Fig. 3. (Top) Amplitude of the first two EOFs ϕ_1 and ϕ_2 for the thermistor string temperature. The first mode does not change sign over the water column. (Bottom) Corresponding expansion coefficients. The first expansion coefficient clearly represents the oscillation of the thermocline in time (compare with 16 °C temperature contour in Fig. 2). Both coefficients have stronger (absolute) values during internal wave events.

"EOFs" refers to the vertical spatial patterns $\phi_i(z)$ and that "expansion/projection coefficient" refers to the temporal patterns or weights $\alpha_i(t)$.

Fig. 3(top) illustrates the first two EOF modes, and Fig. 3(bottom) shows the corresponding principal components. With the inherent efficiency of this statistical description a very few empirical modes are used to describe the fundamental variability in a very large data set; the two first modes for our data set represent 99.5% of the variance. All EOFs are very clean and smooth, representing a dynamical pattern consisting of a background stratification interacting with internal wave occurrence. The amplitude of the first EOF does not change sign over the water column and has one extremum. Therefore, all the isotherms oscillate in the same direction [18] with maximum displacement at 85–90 m. The second EOF has two extrema, as a consequence of the orthogonality constraint, and changes sign close to the first EOF maximum depth. This indicates that isotherms are moving in opposite

directions above and below the pycnocline [18]. The first EOF can be interpreted as a vertical displacement of the thermocline whereas the second one illustrates the change in slope of the temperature gradient. To make sure the physical interpretation is right as the EOF data modes are not necessarily related to physical modes, the corresponding first two projection (expansion) coefficients, illustrated in Fig. 3(bottom), are also plotted. The projection coefficient of EOF1 is negative at the beginning and turns positive after November 6, 2006. Looking at the thermocline on Fig. 2, it is noticeable that the projection coefficient represents exactly the variations of the thermocline, being negative when the thermocline is deeper than its mean depth (EOF1 maximum) and positive when the thermocline is shallower. The two periods identified in Fig. 2 are thus clearly identified in the first expansion coefficient representing the vertical displacement of the thermocline depth.

The second projection coefficient mostly stays positive but the amplitude of its variations is bigger (local extrema) during
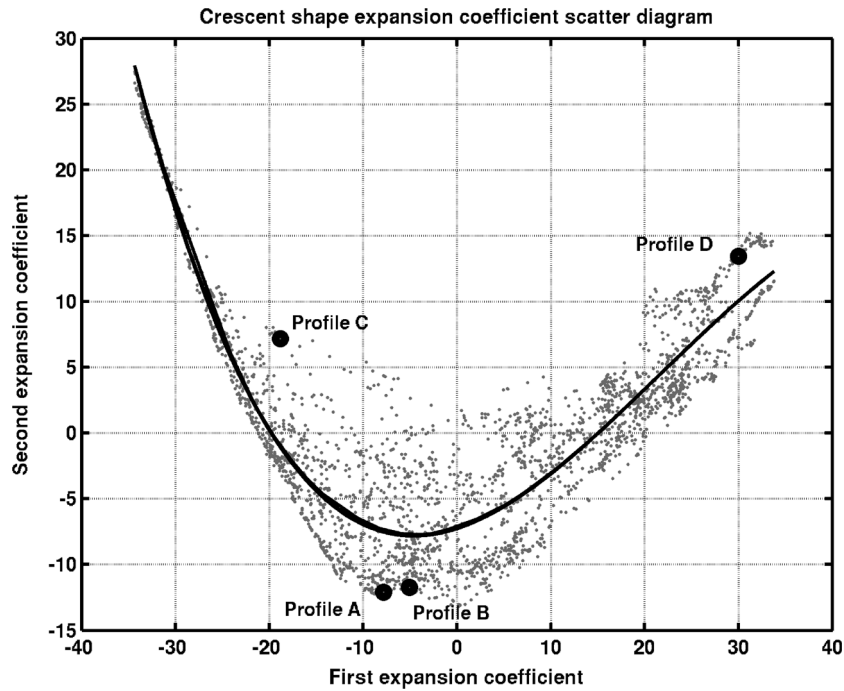
Fig. 4. Scatter diagram formed by plotting the second expansion coefficient versus the first one. The scatter plot has a significant crescent shape illustrating that despite the orthonormal constraints of the EOF analysis, the first two modes are dynamically linked. The letters correspond to the expansion coefficients of the profiles rebuilt in Fig. 5. The black curve represents the fourth-order polynomial fit to the cloud of points.

an internal wave event. All these evidences illustrate that the EOFs, in our case, can be linked to physical modes.

D. Expansion Coefficient Scatter Diagram

As most of the variance was described in the first two EOF modes, the scatter diagram of the first two expansion coefficients was plotted to see if they could be related to an internal wave event [5]. The resulting cloud of points has a crescent shape (Fig. 4) meaning that the two coefficients are not independent: $\alpha_2(t) = f(\alpha_1(t))$.

The IW signal can then be fully described as

$$\psi(z,t) = \bar{\psi} + \alpha_1(t)\phi_1(z) + \alpha_2(t)\phi_2(z) \qquad (2)$$
$$= \bar{\psi} + \alpha_1\phi_1 + f(\alpha_1)\phi_2. \qquad (3)$$

Two regimes can be distinguished on the scatter diagram. In the center of the cloud of points $[|\alpha_1(t)| \prec 15$ and $\alpha_2(t) \prec 0]$, where the cloud of points is thick and dense, $\alpha_1(t)$ takes small values meaning a weak translation of the thermocline depth. $\alpha_2(t)$ is negative, and the corresponding profiles are smooth and typical of a well-stratified water column [5]. This regime represents a "rest regime" with no internal wave events. Looking now at the crescent "branches" with an asymptotic behavior $[|\alpha_1(t)| \succ 15$ and $\alpha_2(t) \succ 0]$, both coefficients increase in a linear correlation. This regime represents typically the internal wave dynamics: when the thermocline is depressed by the interfacial waves [represented by $\alpha_1(t)$], the deviation of the interface generates a horizontal circulation with opposite horizontal currents below and above the interface of the thermocline [gradient variability represented by $\alpha_2(t)$]. These baroclinic currents are added to the external barotropic current. Once the IWT has passed, this baroclinic structure disappears and we are back in the first described regime.

This crescent shape scatter diagram was confirmed by numerical simulations [5] using the nonlinear and nonhydrostatic 2.5 D Lamb model [6].

The crescent-shaped distribution means that the two EOF projection coefficients are dynamically linked. When this result was first published in [5], a lot of questions arose from the reviewers and the scientific community. EOFs are built under some orthogonal constraints: 1) the EOF modes $\phi_i(z)$ are orthogonal in space meaning that there is no correlation between any two EOFs $(\phi_i \cdot \phi_j = \delta_{ij})$ and 2) the expansion coefficient time series $\alpha_i(t)$ is orthogonal in time meaning that there is no simultaneous temporal correlation between any two expansion coefficients $(\alpha_i \cdot \alpha_j = \delta_{ij})$. These two constraints were checked and respected for the first two EOF modes considered here: $\phi_1 \cdot \phi_2 = 0$ and $\alpha_1 \cdot \alpha_2 = 0$. The scatter diagram of the expansion coefficients having a specific shape is not in contradiction with the orthogonality constraint; it only highlights a dynamical interaction between these two modes illustrating that the vertical oscillation of the thermocline during an internal wave event is related to the change in slope of its gradient.

The black curve in Fig. 4 indicates a fourth-order polynomial fit $P(\alpha_1)$ of the scatter diagram and thus the mathematical relation between the first two expansion coefficients. This property was used to rebuild the profiles from the scatter plot polynomial fit and the two vertical EOF modes.

Two other examples of scatter diagrams are displayed in Fig. 5. These are scatter diagrams which were rebuilt from the expansion coefficients of thermistor string temperature time series measured close to the Setubal canyon on the western coast of Portugal during the 2007 Random Array of Drifting Acoustic Receivers (RADAR) trial jointly organized by CINTAL, Algarve, Portugal and Instituo Hidrografico (IH), Lisboa, Portugal, with three other teams from NATO
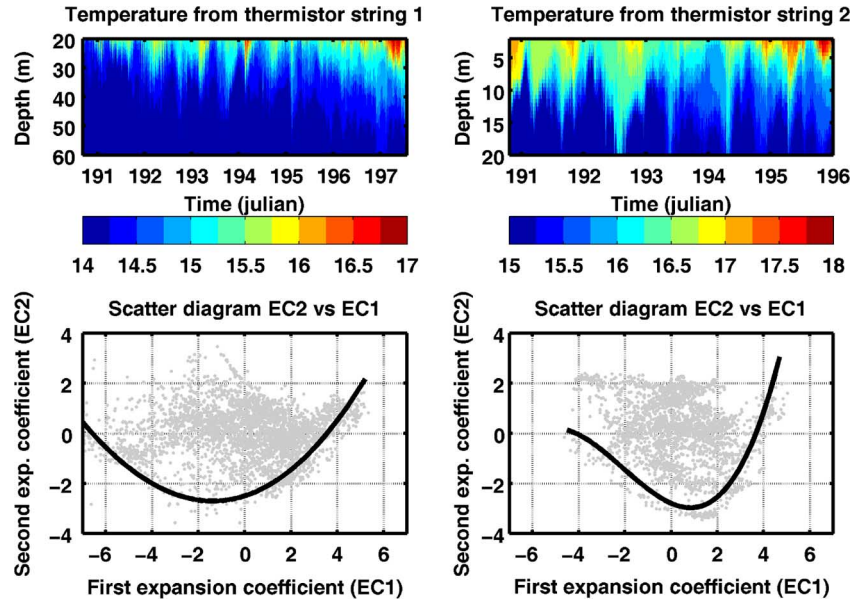
Fig. 5.   Two other examples of scatter plots. The temperature thermistor strings measurements were made during the RADAR'07 trial close to the Setubal canyon on the western coast of Portugal in July 2007. The RADAR'07 trial was jointly organized by CINTAL/SiPLAB and Instituo Hidrografico (IH) with three other teams from NURC, HLS Research, and Navy Research Laboratory (NRL). Their positions are (8°58′6″ W; 38°19′44″ N) for thermistor string 1, and (8°55′37″ W; 38°21′45″ N) for thermistor string 2. The emettor depths of hermistor string 1 ranged from 15 to 99 m with a spacing of 1 m. Thermistor string 2 had 11 emettors ranging from 2 to 22 m by step of 2 m. They were both positioned northward of the Setubal canyon.
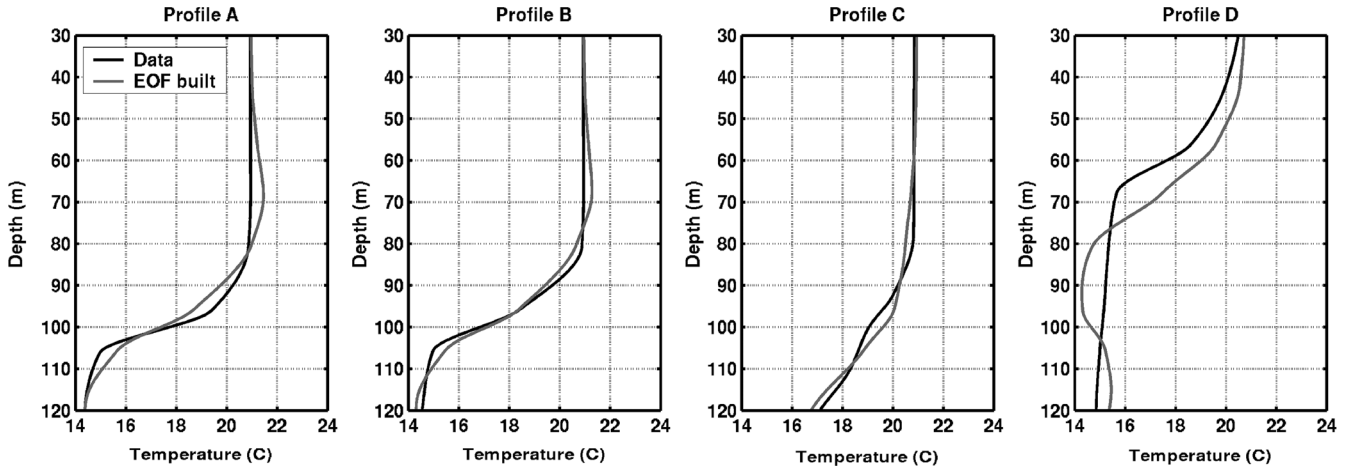

Fig. 6.   Randomly rebuilt temperature profiles from the two first modes of the EOF analysis. In black, original data temperature profiles, in gray, two-mode rebuilt profiles. The profiles are located on the expansion coefficient scatter diagram in Fig. 4.

Undersea Research Centre (NURC), La Spezia, Italy, Navy Research Laboratory (NRL), Stennis Space Center, MS, and Heat, Light and Sound Research (HLS), La Jolla, CA. Their positions are (8°58′6″ W; 38°19′44″ N) for thermistor string 1, and (8°55′37″ W; 38°21′45″ N) for thermistor string 2. The internal wave dynamics here is not as strong as in the Messina Strait (weaker amplitudes) and the dynamics close to the canyon are much more complex. The shape of the cloud of points in both scatter diagrams is not as neat as for Messina Strait. Still the lower limit of the cloud of points is well designed and can, once again, be fitted with a polynomial fit illustrating a dynamical link between both coefficients. This study will go on with the Messina Strait scatter plot, but these latter examples illustrate that our methodology can be derived for several areas with strong dynamics.

III. REPRESENTATION OF TEMPERATURE WITH EOFS

In [5], the EOF analysis was done on the density. As our aim here is to rebuild the temperature profiles for sound-speed profile computation, the EOFs are applied to the temperature measured by the thermistor string. The EOF and the scatter diagram are obviously exactly the same; only the axis scales change.

A. Reconstruction Methodology

As noticed in Section II-C, the variance is fully contained in the first two EOFs (over 99.5%). Moreover, the EOF coefficients are dynamically linked and the whole water column variability can be described by a polynomial function.
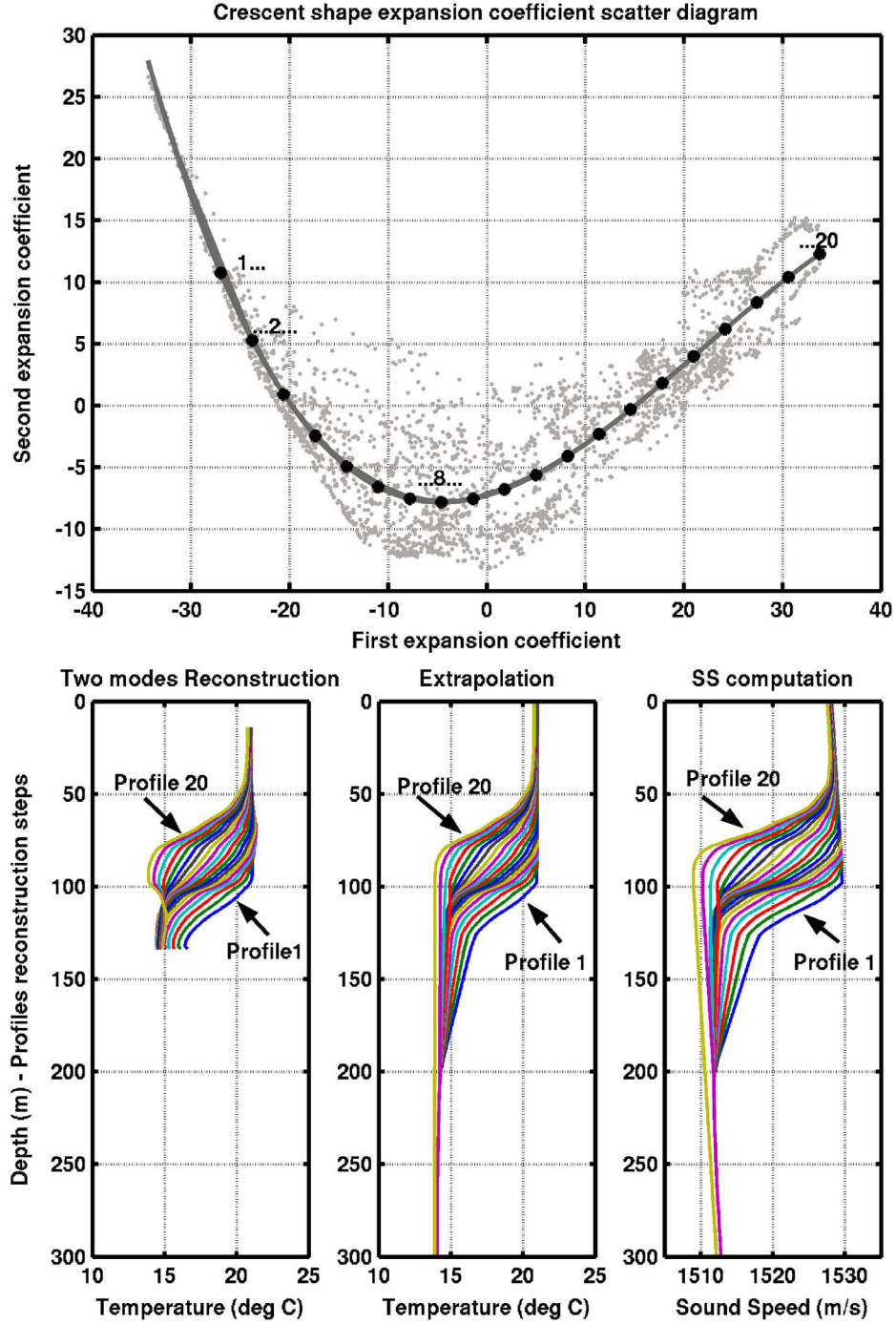
Fig. 7. (Top) Scatter diagram formed by plotting the second expansion coefficient versus the first one. The black dots represent the sampling in 20 profiles of the polynomial fit. The corresponding rebuilt profiles are illustrated below, from the first step of the two-mode reconstruction to the computation of sound speed.

- By choosing a point on the polynomial fit $P(\alpha_1)$ of the scatter diagram, the water column temperature can be reconstructed using

$$T_i(z) = T_{\text{mean}} + \alpha_{1i} * \phi_1(z) + P(\alpha_{1i}) * \phi_2(z),$$
$$\text{for } i = \text{time} \quad (4)$$

where ϕ_1 and ϕ_2 are the EOFs (spatial modes) and α_{1i} and $P(\alpha_{1i})$ are the coefficients at the chosen time i.

Moreover, as the thermistor string data were available between 20- and 130-m depth, the temperature profiles were then extrapolated on the whole water column (steps in Fig. 7).
- For the layer up to the surface, the profile was extended by a constant value corresponding to the shallower value available. As we are in the mixed layer, this approximation is correct.
- From the deepest profile value to the bottom, the profile was extrapolated to a mean temperature profile computed from the deepest CTD measurements. The profiles were

then slightly filtered to smooth the transitions of the different parts of each profile (Fig. 7, middle graph). Four profiles were rebuilt randomly and are indicated in Fig. 4. Profiles A and B are in the "rest regime" where the density of points is most dense. Profiles C and D are located farther along the asymptotes, corresponding more to an internal wave regime. For profiles located in the rest regime (first two graphs in Fig. 6), the reconstruction works well. A slight temperature inversion is observed, most likely due to the very negative values of the second mode expansion coefficient. Unfortunately for the last reconstructed profile [Fig. 6(right)], the result is poor. To compensate for the high thermocline depth (60 m), the expansion coefficients are strong, thus introducing too much variability and a great artefact at the thermocline depth mean position (110 m). This was corrected by a temperature inversion check in the reconstruction routine.

- The temperature inversion check is simple. If the temperature value at level z_{i+1} (deeper) is higher than the temperature at level z_i then the temperature at z_{i+1} is corrected and taken equal to the value at z_i. That simple correction works well as the inversions often appeared in the mixed layer or at the bottom of the thermocline.
- Finally, the sound speed $c_i(z)$ was computed using Medwin formula from [19], function of temperature, salinity (salinity was chosen from data as constant and equal to 38.51), and depth

$$
\begin{aligned}
c_i(z) = {} & 1449.2 + 4.6 \times T_i(z) - 0.055 \times T_i^2(z) + \cdots \\
& 0.00029 \times T_i^3(z) + (1.34 - T_i(z)) \times (S - 35) \\
& + 0.016 \times z.
\end{aligned} \tag{5}
$$

These steps are illustrated in Fig. 7. The sound-speed profiles are now ready to be used as acoustical model inputs.

B. Case 1: Curve Sampling and Systematic Reconstructed Profiles

By sampling the polynomial fit, an exhaustive set of temperature profiles can be reconstructed. The curve was sampled for 20 values of the first principal component. It was chosen not to start at the minimum of the first expansion coefficient as the density of points was very low and most likely insufficient to have the proper shape of the polynomial left branch (Fig. 7).

Once the sampling coefficients were chosen, the 20 sound-speed profiles were reconstructed using the methodology described in the previous paragraph. In 50% of the cases, the fit to the data is very good. The main differences appear for extreme values of α_1 (most likely because of the weaker density of points that may have an impact on the polynomial fit) but also when the gradient of the thermocline is very strong as in profiles 10 and 13. Overall, the fit is good for a two-EOF reconstructed profile.

These profiles illustrate the whole water column variability that can be observed. Applying an acoustic propagation model to these profiles will give an exhaustive representation of the environmental acoustic properties of the Strait (Section IV) without any central processing unit (CPU) consuming ocean modeling.
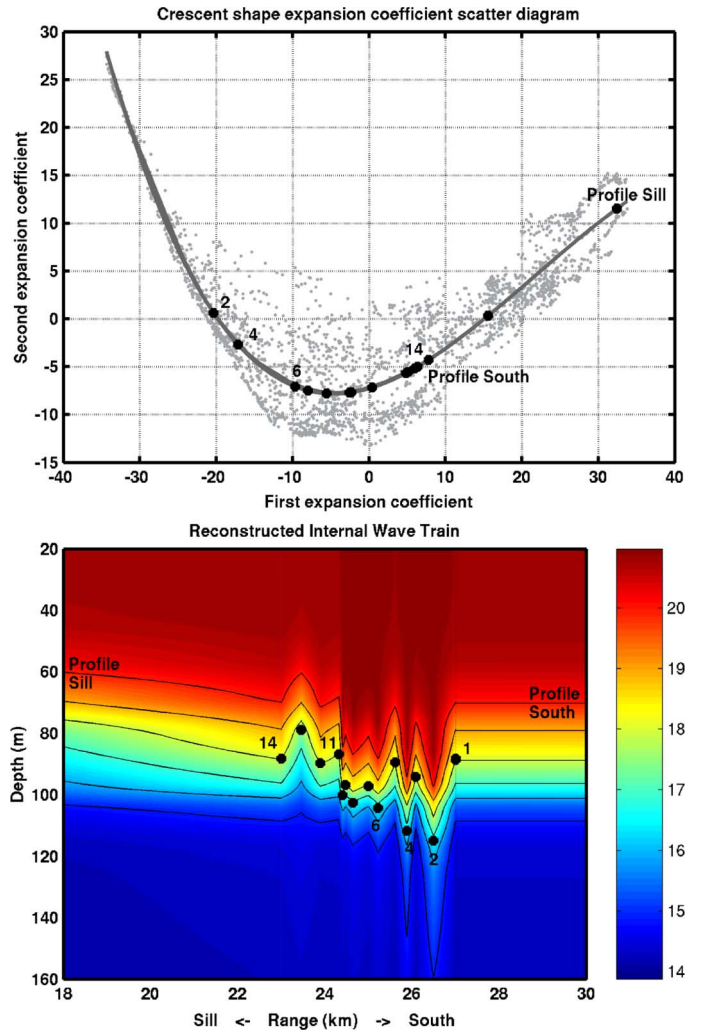

Fig. 8. Reconstruction of an IWT. The color bar indicates the temperature in degrees Celsius. The profiles were chosen on the polynomial fit in order to rebuild an IWT whose characteristics corresponded to the ones identified in [5].

C. Case 2: IWT Reconstruction

In this second case, we have looked at how the polynomial fit was browsed during an IWT event. A wave train was reconstructed in agreement with the IWT characteristics in the Strait of Messina.

Fig. 8 illustrates all the steps from the sampling of the profiles to the reconstruction of the IWT. The rebuilt wave train has four internal waves of maximum amplitude of 30 m in a distance of 4 km. It was rebuilt with 14 profiles.

The profile at the sill is the one that has the shallower thermocline, so it was chosen well on the "right-hand side" (positive first expansion coefficient) of the polynomial. The profile southwards must have a deeper thermocline and was chosen closer to the bottom of the polynomial to have a thermocline about 100 m deep. Concerning now the train itself, points 2, 4, and 6 represent the main waves of the train, and we must then have negative values of the first expansion coefficient to get a deeper thermocline: the values of the first expansion coefficient and thus the
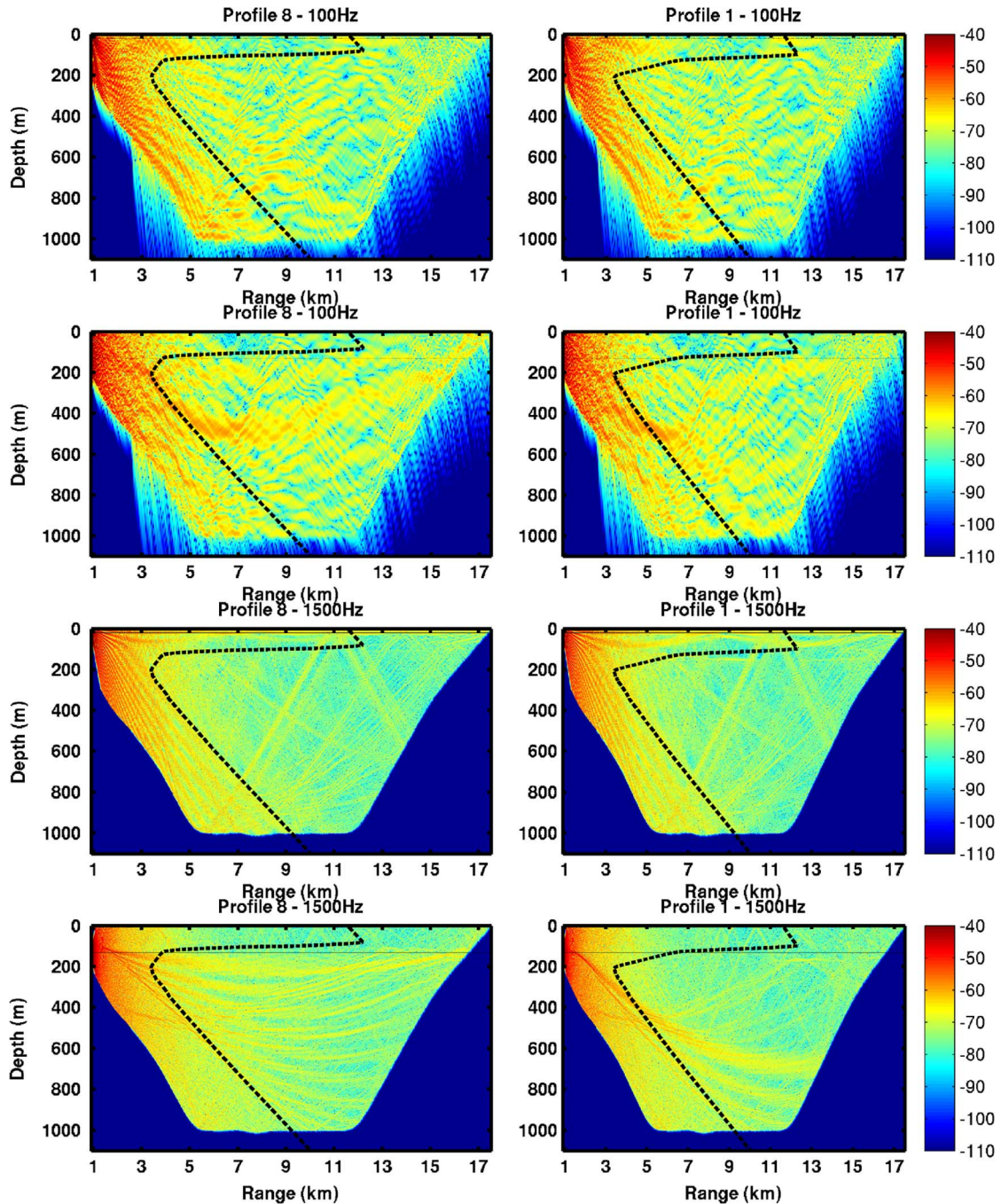
Fig. 9. Two-dimensional transmission loss on the whole water column for $f = 100$ Hz (top) and $f = 1500$ Hz (bottom) for Profile 8 "rest-position" (left column) and Profile 1 "internal wave occurrence" (right column). Color bars indicate the loss in decibels for each configuration. The range goes from the Sicilian coast to the Calabrian coast. On the first and third lines, the source is 20 m deep, and on the second and fourth lines, the source is 130 m deep. The range-independent sound-speed profile is displayed in the graphs in black.

amplitude of each wave are, respectively, 20, 17, and 10 m. Between each wave, the thermocline has to come back to its average depth, so that the profiles are chosen close to the bottom of the polynomial.

Just by using the polynomial function, a wave train can be easily reconstructed and thus a physical feature study can be conducted.

IV. ACOUSTIC PROPAGATION

In this section, we illustrate the methodology by running acoustic simulation across and along the straits with recon-

structed environments. The purpose is not to derive a full acoustic study of propagation in the Strait of Messina but rather to illustrate by examples the potentiality of our reconstruction approach. The acoustical propagation runs are obtained with the range-dependent acoustic model (RAM), developed in [20]. This model, based on split-step Padé resolution of the parabolic equation (PE), allows the use of a wide range of frequencies. It is used hereafter from 50 to 3500 Hz by a step of 200 Hz.

Two configurations were chosen; one was implemented across the strait (transverse configuration with sound-speed profiles described in Case 1 in Section III-B) and the other
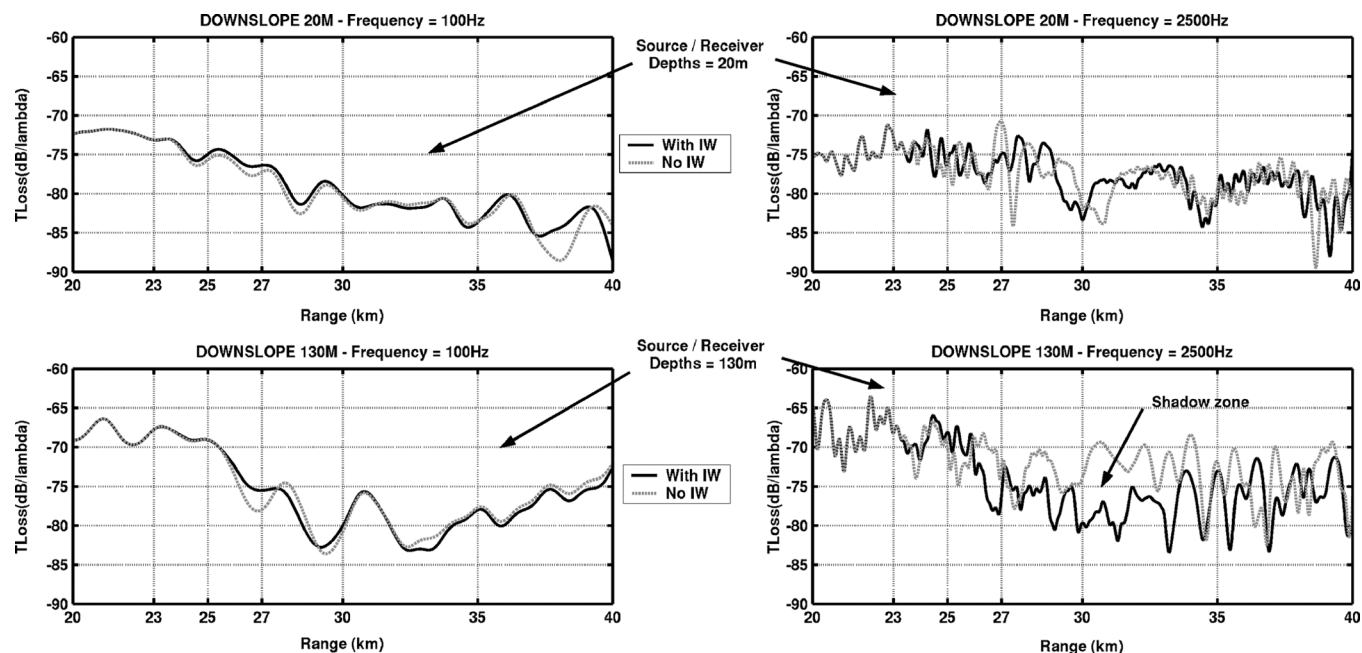
Fig. 10. Transmission loss between a source and a receiver in the axial downslope configuration (along the median of the Strait) for frequencies 100 Hz (left column) and 2500 Hz (right column). Source is positioned 9 km away from the sill (in front of Messina town), and loss is displayed from 20 to 40 km (so that the sill is on the left of the graph and Ionian Sea on the right). The IWT goes from 23 to 27 km. In the first line, the source and the receptor are at the 20-m depth (study of the surface duct). In the second line, the source and the receptor are at the 130-m depth (below the thermocline and the sound-speed minimum).

one followed the median of the strait (axial configuration with sound-speed field described in Case 2 in Section III-C).

- In the configuration transverse to the strait, the source is positioned 900 m away from the Sicilian coast and emits towards the Calabrian coast (16 600-m distance). The scatter plot polynomial is sampled in 20 points and runs were made systematically for every reconstructed profile and every frequency: the sound-speed profile is range independent but not the sediment nature (see below).
- In the axial configuration along the strait median, the source is positioned either in front of Messina (9 km south of the sill) and emits downslope until 40 km south, or 40 km south of the sill and emits upslope towards the sill. The sound-speed field contains a reconstructed IWT and is thus range dependent.

Bottom nature is derived from [21] and from data extracted from SHOM sediment database. For the transverse configuration, the bottom nature is a succession of rocks (from the source to 6 km), coarse sand and silt (until 5 km), silt (until 11 km), and finally coarse sand and silt (until the receiver). For the axial configuration, the bottom consists in a section of coarse sand and silt over the first 9 km and silt elsewhere.

The source depths are, respectively, 20 m (shallow, in the surface duct), 90 m (intermediate, in the thermocline), and 130 m (deep, in the channel).

A. Transverse Configuration

The transverse configuration is based on the Case 1 profile construction. The acoustical model is positioned transverse to the strait, 27 km south of the sill, and the sound-speed profile is range independent. The used profiles are the 20 profiles rebuilt

as explained in Section III-B. For each of these profiles, propagation loss simulations were made for frequencies ranging from 50 to 800 Hz by a step of 50 Hz and from 900 to 3500 Hz by a step of 200 Hz.

An example of transmission loss field is displayed in Fig. 9. Profile 8 is located at the bottom of the scatter diagram (see position and sound-speed profile in Fig. 7), thus corresponding to a "no internal wave/rest position" profile (left column). Profile 1 represents the occurrence of an internal wave event deepening the thermocline (right column). The frequencies displayed are 100 (four top pictures) and 1500 Hz (four bottom pictures). The sound-speed profiles are displayed on each graph. First and third lines represent the transmission loss for a 20-m-deep source, and second and fourth lines represent the transmission loss for a 130-m-deep source.

Several well-known conclusions easily come up.

- Sediment: for the lower frequencies (and thus longer wavelengths), the nature of the sediment can induce bottom loss. Whereas this loss is little for rocky bottoms, the acoustic energy penetrates deeper for softer sediments. For higher frequencies (bottom pictures), the signal does not penetrate at all in the sediment. It also affects the interference patterns at low frequencies. The rays that have first touched the rocky bottom have a much finer interference pattern than the rays reflecting on the silt bottom or being guided in the water column. For the high frequencies, the change in sediment nature has hardly any impact.
- Surface duct: for both sound-speed profiles, the gradient close to the surface is slightly positive because of the isothermal mixed layer. This bit is followed by a strong negative gradient. When the source is positioned in the positive gradient (20-m depth), the curvature of the rays
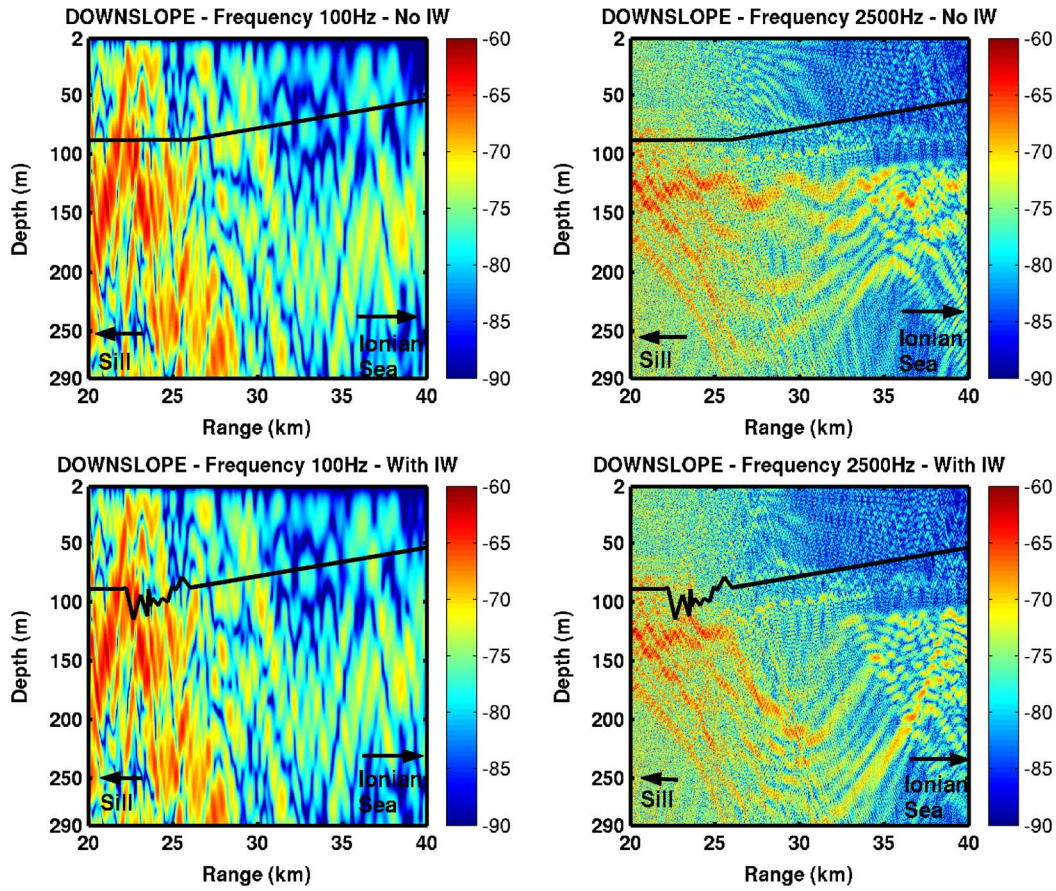
Fig. 11. Two-dimensional transmission loss illustrating the case from Fig. 10 when the source and the receiver are at the 130-m depth, with (top) or without (bottom) IWT. The left column displays the results for the first 300 m of the water column at frequency 100 Hz, and the right column at frequency 2500 Hz. Color bars indicate the transmission loss in decibels.

is upward. The rays with a low angle propagate in this channel by multiple reflections on the surface. The transmission loss is usually quite low if the frequency is neither too low (low-frequency cutoff) nor too high (surface reflection loss). For the 100-Hz run, the energy leaks out of the duct after approximately 4 km. For the 1500-Hz run, the energy is guided through the whole strait.

- Shadow zone: for the 20-m depth source, the rays with a higher angle than the ones propagating in the surface duct are quickly going out of the duct and their curvature is strongly deviated to the bottom because of the strong negative sound-speed gradient. At 1500 Hz, this leaves an important shadow zone which can only be and is insonified by bottom reflected rays (which is less efficient than direct rays). At 100 Hz, the energy leaking out of the surface duct is refracted on the deeper sound-speed positive gradient, which allows a more important insonification of the water column than observed at 1500 Hz. A reinsonification of the surface duct is thus observed at 12 km.
- Deeper source: when the source is placed at 130 m, the surface duct is not insonified anymore except by some geometrically reflected rays. For profile 8, the source immersion is close to the sound-speed minimum. This corresponds to the best insonification possible [SOund Frequency And Ranging channel (SOFAR) propagation type—the SOFAR channel acts as a waveguide for sound

and sound waves within the channel may travel long distances before dissipating] thanks to the absence of reflection loss and the presence of multiple tracks (the only loss is water absorption). It is well illustrated at 1500 Hz. The strait width is too narrow to observe any convergence zone. For profile 1, the source position is under the isothermal zone but still in the thermocline (above the sound-speed minimum). In that case, a huge shadow zone is observed as all the acoustical energy is deviated downward.

This arbitrary example illustrates the different phenomena (surface duct, sofar propagation, sediment impact) that can take place. The results, highly depending on what profile is used, highlight the crucial importance of taking into account internal wave dynamics.

B. Axial Configuration

The reconstructed IWT feature is studied with either the source close to the sill of the strait and emitting towards the open sea (downslope propagation) or the source farther down the strait and emitting towards the sill (upslope propagation).

1) Downslope Propagation: In this configuration, we look at the impact of a complete wave train along the axe of the strait.

The source is positioned in front of Messina (about 9 km south of the sill); the receptor is positioned downslope after the
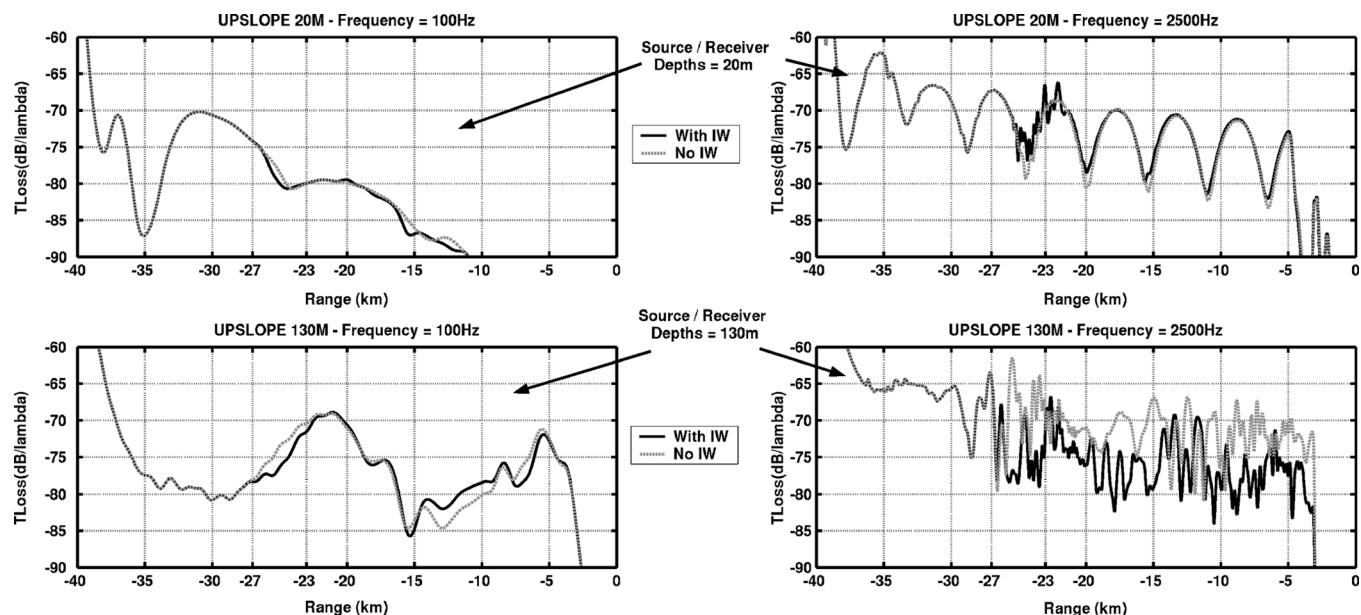
Fig. 12.   Transmission loss between a source and a receiver in the axial upslope configuration (along median of the Strait) for frequencies 100 Hz (left column) and 2500 (right column). Source is positioned 40 km away from the sill (in the Ionian Sea) and emits towards the sill thus facing the IWT. Loss is displayed from -40 to -20 km (so that the sill is on the right of the graph and Ionian Sea on the left; contrary to Fig. 10). The IWT goes from -27 to -23 km. In the first line, the source and the receptor are at the 20-m depth (study of the surface duct). In the second line, the source and the receptor are at the 130-m depth (below the thermocline and the sound-speed minimum).

wave train (40 km away from the strait). The internal wave event takes place from 23 to 27 km.

Transmission loss is displayed versus range in Fig. 10. At low frequencies (left column in Fig. 10), there is hardly any difference between the "internal wave" case and the "no internal wave" case. So the leakage observed in the 2-D graphs is independent from the internal wave presence. Acoustic propagation at low frequencies is dominated by the sediment nature rather than the water column characteristics. At high frequencies (right column in Fig. 10), the IWT impact (extending from 23 to 27 km) is visible right after the event (from 27 to 33 km) when the source is at the depth of the event or deeper (90, not shown, and 130 m).

In general, the presence of an internal wave event increases the transmission loss, up to 10 dB in the case of surface duct configuration or when the source is positioned at the same depth or deeper than the internal wave event for a receptor under the mixed layer (130 m).

To understand better the increased transmission loss in the presence of internal waves for higher frequencies, Fig. 11 displays the 2-D transmission loss at 100 and 2500 Hz for a source 130 m deep for "internal wave" case (bottom line) and "no internal wave" case (top line). Looking at the 2500-Hz simulations (right column of Fig. 11), the IWT is followed by an energy loss at 30 km, which explains the increase of transmission loss in Fig. 10. As the wavelength is very short, the acoustic signal sees the train as one thermocline depression. The rays are refracted towards the bottom thus leading to a shadow zone going from the first solitons at 27–33 km, when the first refracted rays get back to the thermocline. Without this event, the water column is fully insonified as Fig. 11 (top right) shows.

2) Upslope Propagation: The configuration is the same as the previous axial one, but the source is positioned at the end of the strait and emits towards the sill so that the propagation occurs upslope.

Fig. 12 (corresponding to the downslope configuration Fig. 10) shows the same conclusions as for the downslope case, but with much less difference between the simulations with and without internal waves. Fig. 13 illustrates the upslope acoustic propagation for a 130-m-deep source and two frequencies: 100 Hz (left column) and 2500 Hz (right column). As already noticed, there is little impact on low frequencies. On the contrary, at 2500 Hz, the deviation of the direct ray by the leading wave is clearly visible. It is followed by a small shadow zone before the first resurgence. After the wave train the direct ray has disappeared, but as the propagation occurs upslope, the refracted and bathymetry-reflected rays do insonify the water column until the strait and the differences are not as dramatic as they were in downslope configuration.

C. Discussion

The EOF-reconstruction method enables to build data-driven synthetic environment which can be used to model the acoustic propagation as illustrated previously. This enables to conduct parametric studies or statistical studies by multiplying the number of simulated environments and adapting the operational scenarios to the addressed problems (e.g., ASW, tomography experiment design, acoustic communications optimization, marine mammals risk mitigation).

As an illustration, Figs. 14 and 15 give an example of potential tactical aid by covering the whole frequency range summing the differences between the simulations with and without internal waves at each frequency in the axial configuration. Fig. 14 shows that in the upslope case, the acoustic propagation is deviated by the envelop of the IWT so that a quiet area is created below the thermocline (green area). On the opposite side,
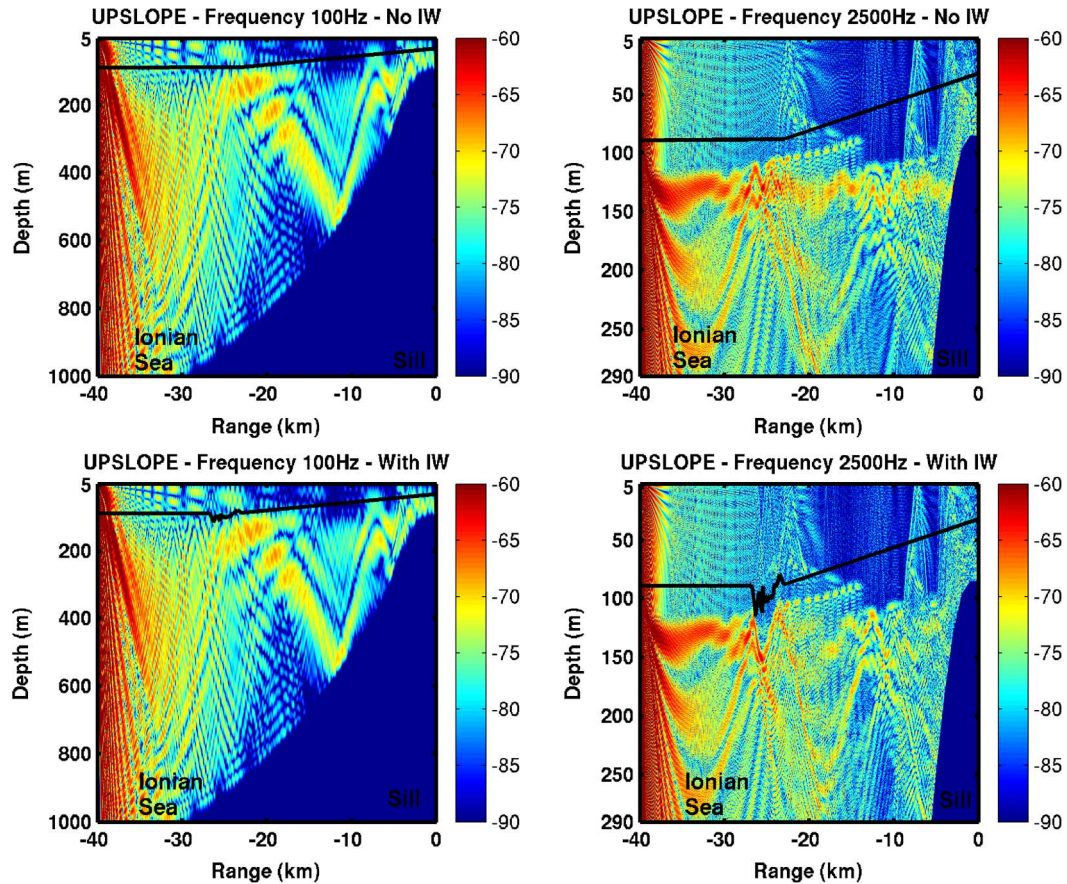
Fig. 13. Two-dimensional transmission loss illustrating the case from Fig. 12 when the source and the receiver are at the 130-m depth, with (top) or without (bottom) IWT. The left column displays the results for the first 1000 m of the water column at frequency 100 Hz (to give the example of the bottom reflections in the upslope configuration), and the right column at frequency 2500 Hz. Color bars indicate the transmission loss in decibels.
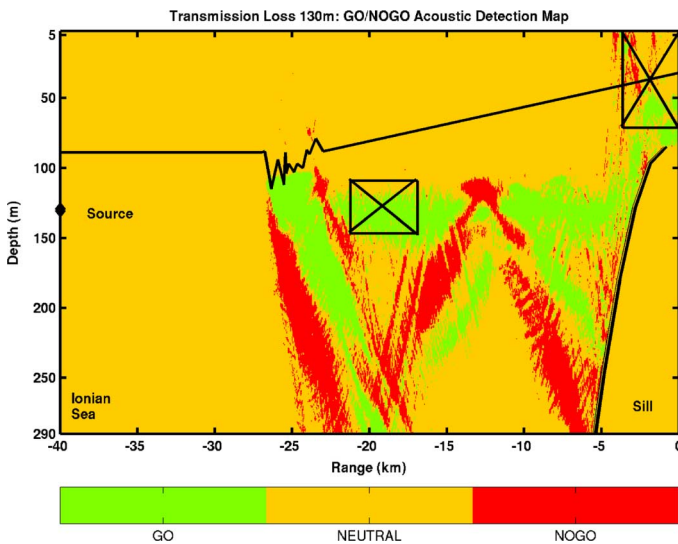

Fig. 14. Upslope qualitative insonification map. The map was obtained by adding all the transmission loss differences between the simulations with internal waves and without, for all frequencies from 50 to 2500 Hz. The green (resp., red) color means the transmission loss with internal wave presence is higher (resp., lower) than without IW.
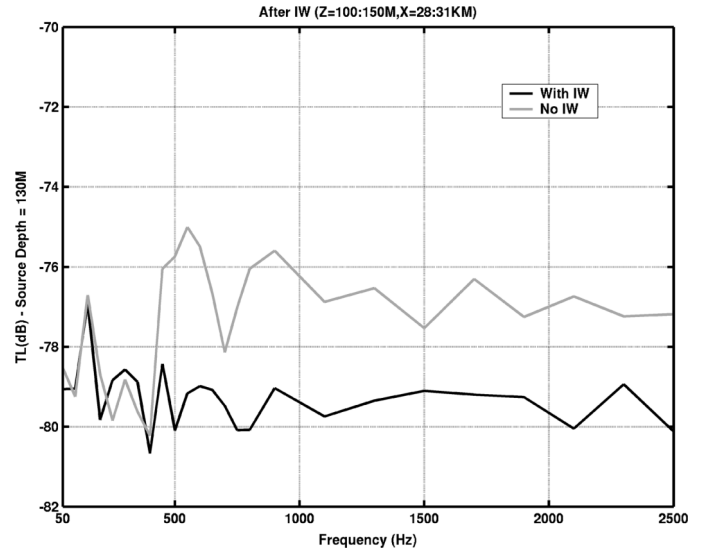
Fig. 15. Transmission loss versus frequency for the axial downslope configuration for a 130-m-deep source. The transmission loss is averaged on the area defined from 28 to 31 km in range and 100–150 m in depth) in the presence of internal waves (black line) and without internal waves (gray line).

other areas (in red) are more likely to be insonified in case of an IWT. Fig. 15 shows that, for the downslope case, low frequencies do not show any impact of the water column physics, but

from 400 Hz and on, the difference becomes important because of the shadow zone induced by the deflection of the rays by the IWT envelop.

These "statistical" outputs summarize the impact of the water column on any frequencies. They are CPU cheap, quickly avail-

able, and can be produced for any scenario, which gives an interesting strategic approach to this methodology.

V. Conclusion

This paper has presented a novel approach to synthesize realistic environments for ocean-acoustic parametric studies. An EOF decomposition is applied to a temporal series of temperature profiles on which it can be observed that the first two time-dependent expansion coefficients are dynamically linked by the internal wave effects. The expansion coefficients plus the polynomial can be used to reconstruct temperature profiles independently from the set of data and can be used to infer the acoustic environment in the area. The methodology presented in this paper is simple to run and requires a very affordable set of data. It could be used as an efficient alternative to ocean and acoustic model coupling for process studies or for regional studies especially in poorly known areas or highly variable areas, where it is difficult to obtain good sound-speed profile prediction from ocean models.

This method could be of great interest for the development of statistical ocean-acoustic decision aids for underwater acoustic operations (e.g., ASW, tomography, communications). Initially a set of data of an area is needed. The statistical analysis gives a polynomial characterization of the dynamics in the area. This could be derived for many areas with strong dynamics. Once this polynomial characterization is established, the users do not need the data anymore (gain of time and memory storage) and can rebuild any possible profile/scenario for physical analysis or statistical tools, possibly through a "blackbox" doing the rebuilding work. An acoustic propagation model can then be coupled to this black box to simulate any desired scenario. Thanks to this method, the simulation of scenarios and the choice of decision aids are in the power of the user who then decides exactly what he needs according to one situation.

The results in the Strait of Messina prove that statistical characterizations of ocean processes could be an interesting tool to replace or more likely complement 3-D ocean-acoustic predictions. Future work will investigate the possibility to extend the EOF reconstruction method to other oceanographic phenomena such as fronts and/or eddies.

References

[1] A. Warn Varnas, S. A. Chin-Bing, D. B. King, Z. Hallock, and J. A. Hawkins, "Ocean-acoustic solitary wave studies and predictions," *Surv. Geophys.*, vol. 24, pp. 39–79, 2003.

[2] A. Warn Varnas, J. Hawkins, P. K. Smolarkiewicz, S. A. Chin-Bing, D. King, and Z. Hallock, "Solitary waves effects north of Strait of Messina," *Ocean Model.*, vol. 18, pp. 97–121, 2007.

[3] Y. Stephan, X. Demoulin, S. Jesus, E. F. Coelho, and M. B. Porter, "Internal tide impact measured by acoustic tomography experiment," *J. Acoust. Soc. Amer.*, vol. 100, no. 4, p. 2613, 1996.

[4] O. Rodriguez, S. Jesus, Y. Stephan, X. Demoulin, M. B. Porter, and E. F. Coelho, "Nonlinear soliton interaction with acoustic signals: Focusing effects," *J. Comput. Acoust.*, vol. 8, no. 2, pp. 347–363, 2002.

[5] G. Casagrande, A. Warn Varnas, Y. Stéphan, and T. Folégot, "Genesis of the coupling of internal wave modes in the Strait of Messina," *J. Mar. Syst.*, vol. 78, no. Suppl. 1, pp. S191–S204, Nov. 2009.

[6] K. Lamb, "Numerical experiments of internal wave generation by strong tidal flow across a finite amplitude bank edge," *J. Geophys. Res.*, vol. 99, no. C1, pp. 843–864, 1994.

[7] W. Alpers and E. Salusti, "Scylla and Charybdis observed from space," *J. Geophys. Res.*, vol. 88, no. C3, pp. 1800–1808, 1983.

[8] F. Bignami and E. Salusti, "Tidal currents and transient phenomena in the strait of Messina: A review," in *The Physical Oceanography of Sea Straits*, ser. NATO ASI. Norwell, MA: Kluwer, 1990, pp. 95–124.

[9] N. Zeilon, "On the tidal boundary waves and related hydrodynamical problems," *Kungl. Svenska Vetenskapsakademiens Handlingar*, vol. 47, no. 4, p. 46, 1912.

[10] P. Baines, "The generation of internal tides by flat-bump topography," *Deep Sea Res.*, vol. 20, pp. 179–205, 1973.

[11] P. Baines, "On internal tide generation models," *Deep Sea Res.*, vol. 29, pp. 307–338, 1982.

[12] R. Del Ricco, "Numerical model of the internal calculation of a strait under the influence of the tides, and its application to the Messina Strait," *Nuovo Cimento Soc. Ital. Fis. C*, vol. 5C, no. 1, pp. 21–45, 1982.

[13] P. Brandt, A. Rubino, W. Alpers, and J. O. Backhaus, "Internal waves in the strait of Messina studied by a numerical model and synthetic aperture radar images from ERS 1/2 satellites," *J. Phys. Oceanogr.*, vol. 27, no. 5, pp. 648–663, 1997.

[14] A. Warn Varnas, J. A. Hawkins, K. G. Lamb, and M. Texeira, "Yellow sea ocean-acoustic solitary wave modelling studies," *J. Geophys. Res.*, vol. 110, 2005, DOI:10.1029/2004JC002801 .

[15] W. Emery and R. Thomson, *Data Analysis Methods in Physical Oceanography*. Amsterdam, The Netherlands: Elsevier, 1997, p. 634.

[16] R. W. Preisendorfer, *Principal Component Analysis in Meteorology and Oceanography*. Amsterdam, The Netherlands: Elsevier, 1988, p. 425.

[17] D. Dommenget and M. Latif, "A cautionary note on the interpretation of EOF," *J. Climate*, vol. 15, no. 2, pp. 216–225, 2002.

[18] A. Vázquez, N. Stashchuk, V. Vlasenko, M. Bruno, A. Izquierdo, and P. C. Gallacher, "Evidence of multimodal structure of the baroclinic tide in the Strait of Gibraltar," *Geophys. Res. Lett.*, vol. 33, no. 17, 2006, DOI: 10.1029/2006GL026806.

[19] H. Medwin and C. S. Clay, , R. Stern and M. Levy, Eds., *Fundamentals of Acoustical Oceanography*. San Diego, CA: Academic, 1998, p. 712.

[20] M. D. Collins, "A split-step Padé solution for the parabolic equation method," *J. Acoust. Soc. Amer.*, vol. 93, pp. 1736–1742, 1993.

[21] V. Santoro, E. Amore, L. Cavallaro, G. Cozzo, and E. Foti, "Sand waves in the Messina Strait, Italy," *J. Coastal Res., Special Issue 36*, pp. 640–653, 2002.

Gaëlle Casagrande received the M.Sc. degree in physics from the Université Paul Sabatier, Toulouse, France, in 2000, the M.Sc. degree in oceanography, meteorology, and environment from the Université de Jussieu, Paris, France, in 2002, and the M.Eng. degree from the French Engineer School ENSTA, Paris, France, in 2002.

Her career started at the French Naval Hydrographic and Oceanographic Institute (SHOM), where she first worked on the coupling of high-resolution meteorological and oceanographic models in coastal areas. She then widened her field of interest by working on joint ocean-acoustic studies and predictions, where she focused on the impact of ocean environment on very low-frequency acoustic propagation for application to antisubmarine warfare. This study evolved to her work on the statistical characterization of internal waves and their impact on acoustic propagation at the MILitary Oceanography department of NATO Undersea Research Centre (NURC, ex-SACLANT), La Spezia, Italy, in collaboration with the American Naval Research Lab (NRL). She coauthored three publications on this joint ocean-acoustics collaboration. She is now at the French General Directorate for Armament (DGA), Paris, France.

Yann Stéphan was born in Lannion, France, in 1966. He received the engineering diploma in electrical engineering from Ecole Nationale Supérieure des Ingénieurs Electriciens de Grenoble (ENSIEG), Grenoble, France, in 1991 and the Ph.D. degree in computer sciences from Conservatoire National des Arts et Metiers (CNAM), Paris, France, in 1996.

Since 1992, he has worked with the Service Hydrographique et Océanographique de la Marine (SHOM) within the Military Oceanography Department, Brest, France. His current interests include acoustic environmental assessment and tactical use of the environment.

Space Center, MS, where he develops internal wave prediction. He has worked jointly on projects with colleagues at Dartmouth College, WHOI, SCRIPPS, Harvard University, University of Massachusetts, University of Waterloo, and the Polytechnic University of Puerto Rico. He has authored and coauthored numerous publications on his work. His interests include internal waves from a cross-disciplinary approach involving joint ocean-acoustic studies and predictions, linking oceanographic and acoustic parameters, ocean model optimization using acoustic modes, water mass and feature models for mesoscale prediction, rapid assessment and prediction of the ocean.

Dr. Warn-Varnas is a member of the American Geophysical Union, European Geophysical Society, Sigma Xi, Oceanographic Society, and the American Acoustical Society.

Alex C. Warn-Varnas received the B.S. degree in physics from the University of Illinois, Chicago, in 1960, the M.S. degree in physics from DePaul University, Chicago, IL, in 1963 and the Ph.D. degree in geophysical fluid dynamics from the University of Notre Dame, Notre Dame, IN, in 1969.

Over the past 36 years, his career involved: engineering work at NASA and General Dynamics & Astronautics; radiation physics at the University of Illinois IRE Hospital; teaching at the University of Illinois College of Pharmacy; GFDI Institute Associate on rotating annulus simulations at Florida State University; physics of collapsing mixed regions at the Naval Research Laboratory in DC; Section Head of Upper Ocean Analysis and Prediction at NORDA where upper ocean prediction evolved; visiting associate professor on the level of no motion reference at the University of Chicago and visiting scholar on multiyear ice cycles at Northwestern University; Branch Head of Hydrodynamics & Thermodynamics at NORDA where operational ice prediction evolved; Head of Applied Oceanography Department at NATO's SACLANT Undersea Research Centre, La Spezia, Italy, where he evolved with colleagues rapid assessment of the mesoscale in the ocean; and oceanographer at the Stennis Naval Research Laboratory, Stennis

Thomas Folegot was born in Lagny, France, in 1970. He received the M.S. degree in mechanics and fluid physics from Ecole Centrale (ECL), Lyon, France, in 1995 and the Ph.D. degree in physical acoustics from "Laboratoire des Ondes et Acoustic," Paris University, Paris, France, in 2003.

In 1996, he started working as a Scientist for the French Military Centre of Oceanography on ocean-acoustic tomography issues before acting as Project Manager for the French Ministry of Defence to design the very first underwater high-frequency time reversal mirror at high frequencies. He has been a Project Manager within the Nato Underwater Research Center from 2003 to 2009, La Spezia, Italy to develop high-frequencies techniques for rapid environmental assessment and for harbor protection. He contributed to three patents in the domain of time-reversal coastal underwater detection, an acoustic barrier, and global ocean noise monitoring and prediction. Since 2009, he has been the founder and president of Quiet-Oceans, Brest, France, which offers to industry and governments services related with the issue of underwater anthropic noise in relation with the emerging regulations and concerns for the marine life.